

Terahertz radiation generation by laser-resonant excitation of terahertz surface magnetoplasmons on a graphene-n-InSb semiconductor interface

Rohit Kumar Srivastav¹ and Mrityunjay Kundu^{1,2,*}

¹*Institute for Plasma Research, Bhat, Gandhinagar 382428, India and*

²*Homi Bhabha National Institute, Anushaktinagar, Mumbai - 400094, India*

(*Corresponding author email:mkundu@ipr.res.in)

(Dated: March 20, 2025)

We propose a method for the laser-excitation of terahertz surface magnetoplasmons via the linear mode conversion of terahertz radiation on a graphene sheet deposited on an n-type semiconductor in presence of an external magnetic field parallel to the semiconductor surface. An obliquely incident p-polarized laser beam interacting with the graphene n-InSb semiconductor surface, imparts linear oscillatory velocity to the free electrons. This oscillatory velocity couples with the modulated electron density to generate a linear current density, which resonantly excites terahertz surface magnetoplasmons. It is shown that the amplitude of terahertz surface magnetoplasmons wave can be tuned by adjusting the external magnetic field (B_0), the graphene's Fermi energy (E_F), the semiconductor's temperature (T), and the incident angle (θ) of laser. This mechanism has the potential to enable the development of an actively tunable plasmonic device.

I. INTRODUCTION

Terahertz (THz) radiation, a kind of electromagnetic (EM) radiation, spans frequencies between 0.1 – 10 THz. Thus it is placed between the infrared and microwave regions of the EM spectrum with wavelength [1, 2] from 1 mm to 30 μm . A unique feature of THz radiation is its ability to penetrate materials like plastic, paper, clothing, and wood materials that are typically opaque to visible lights with minimal energy loss. Many molecules are detectable at THz frequencies due to the strong rotational and vibrational resonances they exhibit [3]. Terahertz technology is now applied in many areas, e.g. explosive and drug detection [4, 5], security screening [6, 7], spectroscopy [8, 9] and medical research [10–13]. Unlike x-rays, which pose health risks, THz devices are known to be safe for non-destructive testing [3].

Radiation of THz frequencies can be generated through linear and nonlinear processes, such as optical rectification [14–16], the beating of two lasers [17–19], and harmonic generation [20], among others. It can also be produced by lasers (or electron beams) interacting with plasmas, metals, semiconductors, or carbon nanotubes [21–25]. Hua *et al.* [26] investigated THz generation by intense laser interaction with two solid layers using particle-in-cell simulation. Chamoli *et al.* [27] studied THz generation over metallic surface by beating of two laser beams in the presence of an external magnetic field. In this case, reported THz frequency ranges $\sim 1 - 4.5$ THz with magnetic fields 10 – 30 T. Also Vij [28] proposed THz generation by Gaussian laser beam interaction with a magnetized carbon nanotube, where magnetic fields of 200 – 500 T were used. Kumar *et al.* [29] explored the effect of external magnetic field over linear mode conversion (LMC) of THz radiation into THz surface plasma waves (SPWs) on a rippled n-InSb semiconductor surface. Recently, Srivastav and Panwar [30] reported THz generation over a graphene (a two-dimensional material with carbon atoms organized in a hexagonal lattice) surface by using LMC of THz radiation into THz SPWs.

The importance of graphene is recognized due to its distinct thermal, optical, mechanical, and electrical character-

istics; and there has been a significant increase in scientific interest in it [31–33]. Graphene holds promise for numerous applications in two-dimensional photonics and plasmonics [34–36]. It can sustain localized EM surface plasmon polariton waves with both TE and TM polarization [37–40]. Graphene-based structures enable strong light-matter interactions owing to their high confinement and extended propagation length [41, 42]. They facilitate the excitation and transmission of surface plasmons (SPs) within the THz spectrum. In contrast to traditional plasmonic materials such as noble metals, graphene exhibits plasmonic resonance within the crucial THz frequency range [43, 44]. Compared to precious metals, graphene SPs demonstrate much stronger confined light field. Furthermore, the properties of graphene SPs can be tailored by varying the electrostatic gate voltage or applying chemical doping [45, 46]. Thus, graphene SPs have been employed in a variety of applications, such as sensors [47], optical modulators [48], and devices for controlling polarization [49]. Metals such as gold and silicon are crucial for SPs in the visible range, but their role is less significant in the THz range due to their high plasma frequencies. A suitable *alternative* for exploring SPs in the THz frequency range is the n-InSb semiconductor and graphene (as in this work), which features an electron density on the order of 10^{23}m^{-3} and 10^{12}m^{-2} respectively, with a corresponding plasma frequency ω_p within the THz range. The strong influence of external magnetic fields on its dispersion relation and the ability to adjust electron density with temperature enhance the potential of semiconductors for generating THz SPs [50]. Notably, the generation of THz radiation over a graphene-n-InSb semiconductor rippled surface under an external magnetic field using LMC has not yet been investigated in detail.

In the present article, we explore the effects of an external magnetic field, the temperature of the n-InSb semiconductor, and the Fermi energy of graphene on the excitation of THz surface magnetoplasmons (SMPs) wave through the interaction of a p-polarized incident laser beam with a rippled graphene-n-InSb semiconductor surface. The external magnetic field is assumed parallel to the semiconductor surface. The graphene layer on the n-InSb semiconduc-

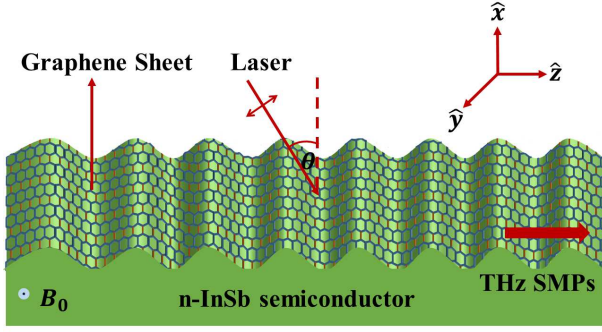


FIG. 1. Schematic of an obliquely incident p-polarized laser beam interacting with a graphene sheet deposited on n-type semiconductor surface in the presence of an external magnetic field $B_0\hat{y}$. The incident angle is θ w.r.t. to the surface normal (dashed line).

tor rippled surface may be developed by chemical vapour deposition or plasma enhanced chemical vapour deposition method [51, 52]. Here, graphene provides additional conductivity σ_g that supports strong SPWs, and the rippled surface provides the extra wave number enabling resonant excitation of THz SMPs wave in a magnetic field. The present configuration with the surface-parallel applied external magnetic field is similar to that considered in the seminal works [53, 54], exhibiting asymmetric wave dispersion. We take the advantage of this effect for the excitation of THz SMPs. However, contrary to the earlier works [53, 54] reported in the relatively high magnetic field and high Fermi-energy regime, we find a parameter space spanning the low magnetic field and low Fermi-energy where respective dispersion curves move in the reverse direction with increasing the magnetic field and Fermi energy, compared to those in Refs. [53, 54] w.r.t. the reference light-line dispersion. This leads to generation of low frequency THz radiations below ~ 6 THz which are useful in many applications. Additionally, our main findings indicate that the amplitude of THz SMPs is tunable by the Fermi energy of graphene, the external magnetic field, the temperature of n-InSb, and the incidence angle of the laser.

The layout of this article is as follows: we derive the expression of linear current density in Sec.II and the wave amplitude of THz SMPs in Sec.III. Discussion on results and conclusion are given in Sec.IV and Sec.V respectively.

II. LINEAR CURRENT DENSITY: THE SOURCE OF THz

We assume that the graphene-n-InSb semiconductor rippled surface is modulated with the perturbed electron density $n = (n_0/2) + n_q$, $qa \geq 1$ where $n_q = (n_0/2)\cos qz$, q is ripple wave number and a is ripple amplitude [29]. The graphene conductivity is $\sigma_g = (ie^2E_F)/(\pi\hbar^2(\omega_0 + i\nu))$ in the THz frequency regime where graphene's Fermi energy $E_F \gg \hbar\omega_0$ [55, 56], e is the charge of an electron, \hbar is the reduced Planck constant, ω_0 is the incidence light frequency and ν is the average collision frequency of electrons. In an external magnetic field $B_0\hat{y}$, the permittivity of n-InSb semiconductor becomes a tensor $\vec{\epsilon}$ [57]. Its components are $\epsilon_{xx} = \epsilon_{zz} = \epsilon_r - \epsilon_r(\omega_p^2(\omega_0 + i\nu))/\omega_0((\omega_0 + i\nu)^2 - \omega_{ce}^2) - \epsilon_r(\omega_p^2/\omega_0(\omega_0 + i\nu))$, where $\omega_{ce} = eB_0/m_e^*$ is the electron cyclotron frequency, $\omega_p = \sqrt{n_0e^2/m_e^*\epsilon_r\epsilon_0}$ is the electron plasma frequency, $m_e^* = 0.014m_e$ is the effective mass of a free electron, ϵ_r is the permittivity of n-InSb semiconductor, $n_0 = 5.76 \times 10^{20}T^{3/2}\exp(0.26/k_B T)$ is the free electron charge density, k_B is the Boltzmann constant and T is the temperature of n-InSb semiconductor [58, 59]. Here, $\omega_0 > \omega_p$ so plasma is under-dense.

A p-polarized laser of frequency ω_0 and wave numbers k_{0x} , k_{0z} along \hat{x} and \hat{z} respectively, impinges at an angle θ onto the rippled surface of graphene-n-InSb semiconductor as illustrated in Figure 1. The external magnetic field of strength B_0 acts along \hat{y} over the n-InSb semiconductor. The corresponding electric field of amplitude E_0 obeys

$$\vec{E} = E(\hat{z} + \tan\theta\hat{x})e^{-i(\omega_0 t + k_{0x}x - k_{0z}z)} \quad (1)$$

where $E = E_0 \cos\theta$, $k_{0x} = k_0 \cos\theta$, $k_{0z} = k_0 \sin\theta$, $k_0 = \omega_0/c = \sqrt{k_{0x}^2 + k_{0z}^2}$ is the free space amplitude of wave vector, and c is the light speed. The incident light is partially transmitted and reflected. Under these conditions, the resultant electric field of the transmitted wave can be expressed as

$$\vec{E}_T = E_0 T_{tr}(\hat{z} + \beta\hat{x})e^{\alpha x}e^{-i(\omega_0 t - k_{0z}z)} \quad (2)$$

where $\beta = (\epsilon_{xz}\alpha + \epsilon_{xx}ik_{0z})/(-\epsilon_{xx}\alpha + \epsilon_{xz}ik_{0z})$ for $x \leq 0$, $\alpha^2 = k_{0z}^2 - (\omega^2/c^2)\epsilon_{eff}$, $\epsilon_{eff} = (\epsilon_{xx}^2 + \epsilon_{xz}^2)/\epsilon_{xx}$ and $T_{tr} = (2E_0 \cos\theta)/((1 + (\epsilon_{eff}\beta)/\tan\theta)\epsilon_0 + (\sigma_g \cos\theta)/c)$ is the transmission coefficient. Clearly, the graphene's contribution enters through σ_g via T_{tr} .

The incident laser beam when interacts with the graphene-n-InSb semiconductor surface, ionizes their atoms, and creates free electrons. Each of these electrons acquires a linear oscillatory velocity (in the first order approximation)

$$\vec{V} = \frac{e}{m_e^*}(\tilde{v}_x\hat{x} + \tilde{v}_z\hat{z})T_{tr}E_0e^{\alpha x}e^{-i(\omega_0 t - k_{0z}z)} \quad (3)$$

where, $\tilde{v}_x = (\omega_{ce} - i(\omega_0 + i\nu)\beta)/((\omega_0 + i\nu)^2 - \omega_{ce}^2)$ and $\tilde{v}_z = (\omega_{ce}\beta - i(\omega_0 + i\nu))/((\omega_0 + i\nu)^2 - \omega_{ce}^2)$. The velocity \vec{V} couples with the modulated electron density n_q , leading to an oscillatory electron current density

$$\vec{J}_\omega^l = -(1/2)n_q e\vec{V} = (\tilde{J}_\omega^x\hat{x} + \tilde{J}_\omega^z\hat{z})T_{tr}E_0e^{\alpha x}e^{-i(\omega t - k_z z)} \quad (4)$$

that propagates with a modified propagation constant $k_z = k_{0z} + q$, and frequency $\omega = \omega_0$. The components of \vec{J}_ω^l are $\tilde{J}_\omega^x = -(1/2)((n_0e^2)/m_e^*)\tilde{v}_x$, $\tilde{J}_\omega^z = -(1/2)((n_0e^2)/m_e^*)\tilde{v}_z$. This current density \vec{J}_ω^l acts as a source of THz.

III. TERAHERTZ GRAPHENE SURFACE MAGNETOPLASMONS WAVE: DISPERSION, AMPLITUDE

The electron current density \vec{J}_ω^l evolves THz SMPs at a frequency $\omega = \omega_0$ and propagation constant $k_z = k_{0z} + q$ in the rippled region. The current source localized in the rippled region may be represented by a delta function $\delta(x)$ [60]. Using the Faraday's law $\vec{\nabla} \times \vec{E} = -(\partial\vec{B}/\partial t)$ and Ampere's law

$\vec{\nabla} \times \vec{B} = \mu_0 \vec{J}_\omega^l + \mu_0 \epsilon_0 \epsilon_r (\partial \vec{E} / \partial t)$, the equation governing the THz SMPs wave can be given as

$$\vec{\nabla}^2 \vec{E} - \vec{\nabla}(\vec{\nabla} \cdot \vec{E}) - \frac{\omega^2}{c^2} (\bar{\epsilon} \vec{E}_\omega) = -\mu_0 i \omega \vec{J}_\omega^l h \delta(x). \quad (5)$$

Here, h is the ripple height, $\bar{\epsilon}$ is the effective permittivity of n-InSb semiconductor (at a frequency ω) with components $\epsilon_{xx} = \epsilon_{zz} = \epsilon_r - \epsilon_r \omega_p^2 (\omega + i\nu) / [\omega((\omega + i\nu)^2 - \omega_{ce}^2)]$, $\epsilon_{xz} = -\epsilon_{zx} = -i\epsilon_r \omega_p^2 \omega_{ce} / [\omega((\omega + i\nu)^2 - \omega_{ce}^2)]$, $\epsilon_{yy} = \epsilon_r - \epsilon_r \omega_p^2 / [\omega(\omega + i\nu)]$, $\epsilon_{xy} = \epsilon_{yx} = \epsilon_{yz} = \epsilon_{zy} = 0$ and $\epsilon_{eff} = (\epsilon_{xz}^2 + \epsilon_{zx}^2) / \epsilon_{xx}$. From Eq. (5) we obtain

$$\begin{aligned} \frac{\partial^2 E_\omega^z}{\partial x^2} - \left(k_z^2 - \frac{\omega^2}{c^2} \epsilon_{eff} \right) E_\omega^z = -\frac{c^2 \mu_0 i}{\omega \epsilon_{xx}} \left[\left(\frac{\omega^2}{c^2} \epsilon_{xx} - k_z^2 \right) \tilde{J}_\omega^z \right. \\ \left. + \left(\frac{\omega^2}{c^2} \epsilon_{xz} + i k_z \frac{\partial}{\partial x} \right) \tilde{J}_\omega^x \right] h \delta(x) \quad (6) \end{aligned}$$

Making right-hand side of Eq. (6) zero, the electric field for THz SMPs can be expressed as

$$\vec{E} = E_l e^{-i(\omega t - k_z z)} \begin{cases} (\hat{z} + \beta_1 \hat{x}) e^{-\alpha_1 x}, & \text{air } x > 0 \\ (\hat{z} + \beta_2 \hat{x}) e^{\alpha_2 x}, & \text{graphene-n-InSb } x \leq 0 \end{cases} \quad (7)$$

where, E_l is the amplitude of THz SMPs wave, $\beta_1 = -ik_z / \alpha_1$, $\alpha_1^2 = k_z^2 - (\omega^2 / c^2)$, $\beta_2 = (\epsilon_{xz} \alpha_2 + \epsilon_{xx} ik_z) / (-\epsilon_{xz} \alpha_2 + \epsilon_{xx} ik_z)$, and $\alpha_2^2 = k_z^2 - (\omega^2 / c^2) ((\epsilon_{xz}^2 + \epsilon_{xx}^2) / \epsilon_{xx})$. Here α_1 and α_2 are decaying constants. From $\vec{\nabla} \times \vec{E} = -(\partial \vec{B} / \partial t)$, the associated magnetic field of THz SMPs can be written as

$$\vec{H} = E_l e^{-i(\omega t - k_z z)} \hat{y} \begin{cases} i \frac{\omega \epsilon_0}{\alpha_1} e^{-\alpha_1 x}, & \text{air } x > 0 \\ \frac{i \epsilon_0 \omega \epsilon_{eff} \epsilon_{xx}}{-\epsilon_{xz} \alpha_2 + \epsilon_{xx} ik_z} e^{\alpha_2 x}, & \text{graphene-n-InSb } x \leq 0 \end{cases} \quad (8)$$

Using the jump conditions $\vec{H}_{2,y} - \vec{H}_{1,y} = \vec{J}_{\sigma_g}$ at $x = 0$, where $\vec{J}_{\sigma_g} = \sigma_g \vec{E}_z$; the dispersion relation of THz SMPs reads as [53]

$$\frac{\epsilon_{eff} \epsilon_{xx}}{\epsilon_{xx} \alpha_2 - \epsilon_{xz} ik_z} + \frac{1}{\alpha_1} = \frac{\sigma_g}{i \omega \epsilon_0} \quad (9)$$

For convenience, from Eq.(9), it is customary to plot the wave dispersion curves with the normalized THz frequency $\Omega (= \omega / \omega_p)$ vs normalized wave number $K_z (= k_z c / \omega_p)$. Figure 2 shows the dispersion curves of THz SMPs for different values of graphene Fermi energy $E_F = 80 - 1000$ meV at a normalized value of electron cyclotron frequency $\Omega_{ce} (= \omega_{ce} / \omega_p) = 0.1$ (747 Gauss). It is found that dispersion curves *first move away* from the dispersion curve of the EM wave in free space (called the light-line, LL) with *increasing* E_F , then *reverses toward* the LL for higher value of $E_F \rightarrow 1000$ meV. Results with higher values of $E_F \rightarrow 1000$ meV are similar to those in Refs.[53], particularly above $E_F \sim 400$ meV.

We now concentrate on results with lower values of graphene Fermi energy E_F and magnetic fields. Figure 3a shows the dispersion curves of THz SMPs for four different values of $E_F = 20 - 110$ meV at a normalized electron cyclotron frequency $\Omega_{ce} (= \omega_{ce} / \omega_p) = 0.04$. Similarly, Figure 3b shows the dispersion curves of THz SMPs for four values of $\Omega_{ce} = 0.0 - 0.12$ at a fixed $E_F = 110$ meV. It is clear that

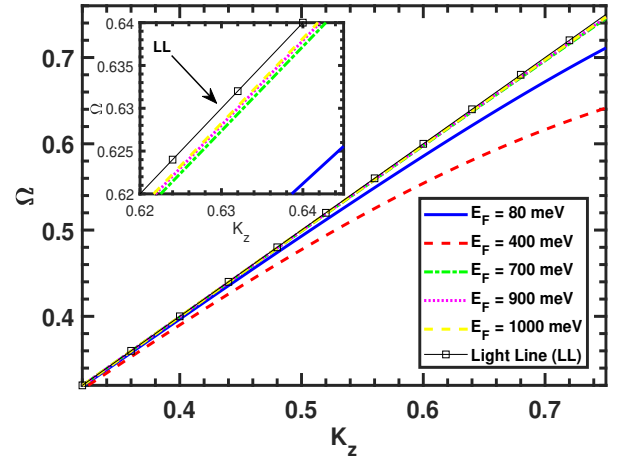


FIG. 2. Wave dispersion curves with the normalized THz frequency $\Omega (= \omega / \omega_p)$ vs normalized wave number $K_z (= k_z c / \omega_p)$ for different values of graphene Fermi energy $E_F = 80 - 1000$ meV at a fixed value of normalized electron cyclotron frequency $\Omega_{ce} (= \omega_{ce} / \omega_p) = 0.1$ (747 Gauss). Line with (\square) is the dispersion curve of EM wave in vacuum (light-line, LL). Inset shows an enlarged view for clarity.

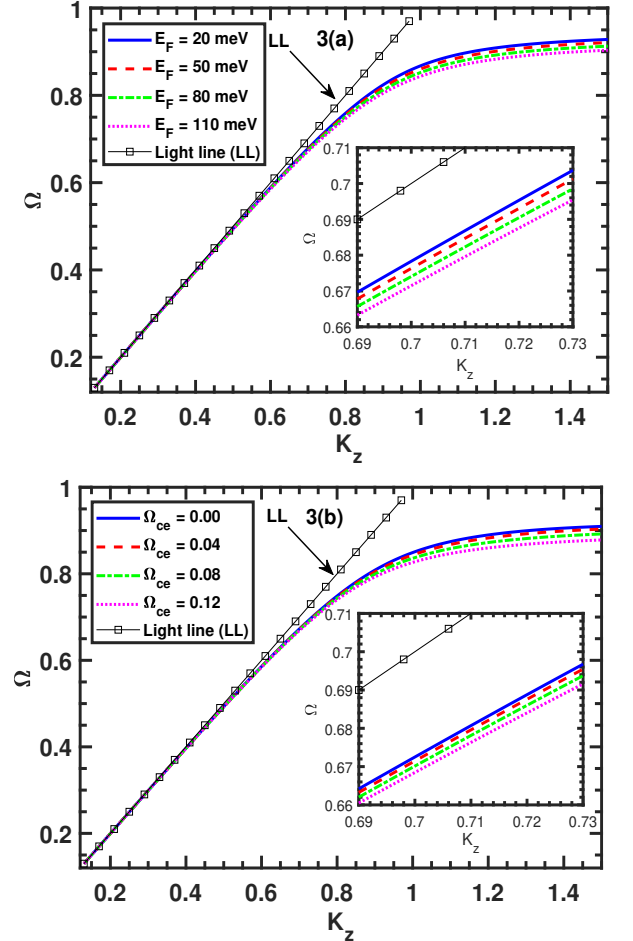


FIG. 3. Wave dispersion curves with the normalized THz frequency $\Omega (= \omega / \omega_p)$ vs normalized wave number $K_z (= k_z c / \omega_p)$: (a) for four values of graphene Fermi energy $E_F = 20$ meV, 50 meV, 80 meV, 110 meV at a fixed value of $\Omega_{ce} (= \omega_{ce} / \omega_p) = 0.04$; and (b) for four values of $\Omega_{ce} = 0.0, 0.04, 0.08$ and 0.12 at a fixed $E_F = 110$ meV. Line with (\square) is the dispersion curve of EM wave in vacuum (light-line, LL). Inset shows an enlarged view for clarity.

the dispersion curve of THz SMPs systematically *shifts away* from the dispersion curve of the EM wave in free space (the light-line, LL) for *increasing* E_F and/or Ω_{ce} – this is a feature that are opposite in nature w.r.t. those presented in Figure 2 with higher values of E_F and Ω_{ce} . The dispersion curves (Figures 3a and 3b) serve as a key analytical tool for characterizing the propagation features of graphene SMPs, especially in configurations involving a n-InSb semiconductor substrate, thereby providing essential insights into their SMPs response.

The excitation of TH SMPs requires phase matching condition

$$q = k_z - k_{0z} \quad (10)$$

with the ripple wave number q . Figure 4a shows the normalized ripple wave number $Q = qc/\omega_p$ versus normalized THz frequency $\Omega (= \omega/\omega_p)$ for four different values of $E_F = 20 - 110$ meV at a fixed value of $\Omega_{ce} = 0.04$ and incident angle $\theta = 30^\circ$. Similarly, Figure 4b shows Q versus Ω for four different values of $\Omega_{ce} = 0.0 - 0.12$ at a fixed $E_F = 110$ meV and $\theta = 30^\circ$. Figure 4c represents Q versus Ω for $\theta = 15^\circ, 30^\circ, 45^\circ$ and 60° at a fixed $E_F = 110$ meV and $\Omega_{ce} = 0.04$. We employ the same numerical parameters that have been previously used for laser interactions with graphene or semiconductor for generating SPs [29, 30]. The present SMPs dispersion curves (Figures 3 and 4) also align with the trend observed in the dispersion curve reported by Liu *et al.* [53] with SPs. Since $q \propto k_z$, results in Figures 4a, b are almost quantitatively similar to those in Figures 3a, b respectively. Additional feature in dispersion is brought out with the angular dependence shown in Figure 4c.

A. Approximate terahertz SMP field

When the current density is finite, the right-hand side of Eq.(6) is also finite. We assume that the mode structure of THz SMPs remains constant [29], while the amplitude of THz SMPs varies as a function of z . Under these conditions, we seek for a solution of the form

$$\vec{E} = E_l(z)\vec{\psi}(x)e^{-i(\omega t - k_z z)} \quad (11)$$

where,

$$\vec{\psi}(x) = \begin{cases} (\hat{z} + \beta_1 \hat{x}) e^{-\alpha_1 x}, & \text{air } x > 0 \\ (\hat{z} + \beta_2 \hat{x}) e^{\alpha_2 x}, & \text{graphene-n-InSb } x \leq 0 \end{cases}$$

Letting $k_z \rightarrow (k_z - i\partial/\partial z)$, and using WKB approximation in Eq.(6) with Eq.(11), we obtain

$$2k_z \vec{\psi}(x) \frac{\partial E_l}{\partial z} e^{-i(\omega t - k_z z)} = -\frac{c^2 \mu_0}{\omega \epsilon_{xx}} \left[\left(\frac{\omega^2}{c^2} \epsilon_{xx} - k_z^2 \right) \times \hat{J}_\omega^z \hat{z} + \left(\frac{\omega^2}{c^2} \epsilon_{xz} + ik_z \alpha_2 \omega \right) \hat{J}_\omega^x \hat{x} \right] h \delta x \quad (12)$$

Multiplying Eq.(12) by $\vec{\psi}^*(x) dx$ and integrating from $-\infty$ to $+\infty$, we obtain

$$2k_z \frac{\partial E_l}{\partial z} e^{-i(\omega t - k_z z)} = -\frac{c^2 \mu_0}{\omega \epsilon_{xx}} \frac{1}{I_1} \left[I_2 \left(\frac{\omega^2}{c^2} \epsilon_{xx} - k_z^2 \right) + \left(\frac{\omega^2}{c^2} \epsilon_{xz} + ik_z \alpha_2 \omega \right) I_3 \right] \quad (13)$$

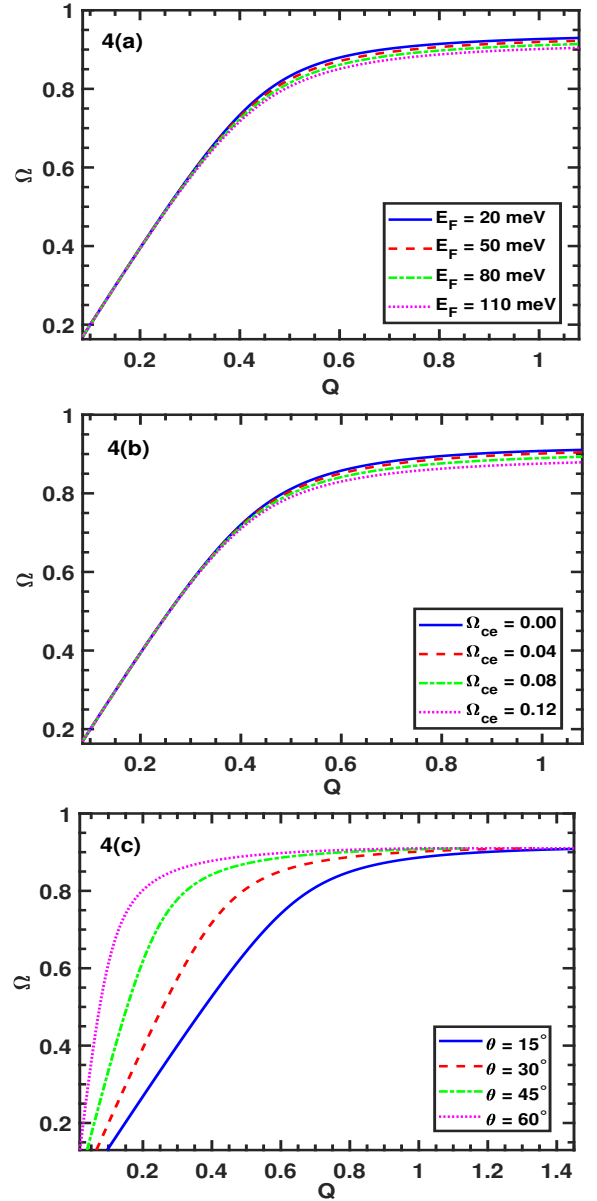


FIG. 4. Dispersion curves with normalized ripple wave number $Q = qc/\omega_p$ versus normalized THz SMPs frequency $\Omega (= \omega/\omega_p)$: (a) for four values of graphene Fermi energy $E_F = 20$ meV, 50 meV, 80 meV and 110 meV at a fixed value of incident angle $\theta = 30^\circ$ and $\Omega_{ce} = 0.04$; (b) for four values of $\Omega_{ce} = 0.0 - 0.12$ at a fixed value of $E_F = 110$ meV and $\theta = 30^\circ$; and (c) for four values of $\theta = 15^\circ, 30^\circ, 45^\circ$ and 60° at a fixed value $E_F = 110$ meV and $\Omega_{ce} = 0.04$.

where, $I_1 = \int_{-\infty}^{\infty} \vec{\psi}^*(x) \cdot \vec{\psi}(x) dx$, $I_2 = \int_{-\infty}^{\infty} \vec{\psi}^*(x) \cdot \hat{J}_\omega^z h \delta x \hat{z} dx$ and $I_3 = \int_{-\infty}^{\infty} \vec{\psi}^*(x) \cdot \hat{J}_\omega^x h \delta x \hat{x} dx$. By integrating Eq.(13) concerning z over the illumination length d , we determine the amplitude of the THz SMPs to be

$$\left| \frac{E_l}{E_0} \right| = \left| \frac{i\omega_p^2}{2k_z \omega \epsilon_{xx}} \left(\frac{1 + \beta_1^2}{\alpha_1} + \frac{1 + \beta_2^2}{\alpha_2} \right)^{-1} \left[2 \left(\frac{\omega^2}{c^2} \epsilon_{xx} - k_z^2 \right) \tilde{v}_z + \left(\frac{\omega^2}{c^2} \epsilon_{xz} + ik_z \alpha_2 \right) (\beta_1^* + \beta_2^*) \tilde{v}_x \right] T_{lr} h d \right|. \quad (14)$$

Equation (14) represents the ratio of THz SMP field strength E_l with incident laser field strength E_0 . It is directly proportional to the transmission coefficient T_{rr} , ripple height h and illumination length d . Results are shown in Sec.IV.

IV. RESULTS AND DISCUSSION

For illustration of variation of THz SMPs field amplitude $|E_l/E_0|$, we choose the CO₂ laser with wavelength $\lambda = 10.81\mu m$ and intensity $I_0 = 2 \times 10^{15} W/cm^2$. The collision frequency $\nu = 0$, illumination length $d = 10\mu m$, ripple height $h = 10\mu m$, n-InSb semiconductor's relative permittivity $\epsilon_r = 15.68$, electron density $n_0 = 2.4 \times 10^{23} m^{-3}$, electron plasma frequency $\omega_p = 9.38$ THz are kept fixed. The normalized THz frequency Ω vary from 0.1 to 0.5, normalized electron cyclotron frequency Ω_{ce} vary from 0 to 0.12, graphene Fermi energy E_F vary from 20 meV to 140 meV. These numerical parameters have also been used previously for laser interactions with graphene or semiconductor, relevant for generating SPs (or SMPs) [29, 30, 61] and also results in Sec.III.

Figure 5 represents normalized THz SMPs field amplitude $|E_l/E_0|$ versus Ω_{ce} for different values of THz frequency $\omega = 2$ THz, 3 THz, 4 THz and 5 THz at a fixed value of $E_F = 120$ meV and $\theta = 82.83^\circ$. It is shown that THz SMPs field amplitude $|E_l/E_0|$ decreases with increasing Ω_{ce} . This is due to the restricted motion of electrons with increasing external magnetic field.

Figure 6 shows $|E_l/E_0|$ versus E_F for different values of THz frequency $\omega = 2$ THz, 3 THz, 4 THz and 5 THz at a fixed $\Omega_{ce} = 0.04$ and $\theta = 82.83^\circ$. The THz SMPs field amplitude $|E_l/E_0|$ is shown to increase with increase in E_F for each ω .

Figure 7 shows $|E_l/E_0|$ versus incident angle θ for different values of THz frequency $\omega = 2$ THz, 3 THz, 4 THz and 5 THz at a fixed $\Omega_{ce} = 0.04$ and $E_F = 120$ meV. The THz SMPs field amplitude $|E_l/E_0|$ increases with increasing θ , reaches a maximum for $\theta \rightarrow 90^\circ$ (grazing incidence) depending upon the ω values, and then it decreases with further increase in θ . It suggests that effects are pronounced near $\theta \approx 83^\circ$ due to linear resonance. At normal incidence no THz is generated. Thus an angle $\theta = 82.83^\circ$ is chosen in Figures 5 and 6 to obtain the maximum effect.

Figure 8 shows $|E_l/E_0|$ versus Ω_{ce} for four different values of n-InSb semiconductor temperature $T=300$ K, 320 K, 340 K and 360 K with a fixed value of $E_F = 120$ meV, THz frequency $\omega = 5$ THz and $\theta = 82.83^\circ$. The THz SMPs field amplitude $|E_l/E_0|$ decreases with increase in Ω_{ce} for $T = 300 - 360$ K as in Figure 5. It suggests that a low magnetic field and higher temperature may lead to higher THz field intensity. It has been previously reported [50] that use of a p-polarized laser beam in an optical rectification mechanism results in THz SPs radiation with a normalized amplitude $|E_l/E_0| \approx 10^{-4}$. In the present work we use LMC process to generate THz radiation on a graphene-n-InSb semiconductor surface in the presence of an external magnetic field, leading to almost 100 times increase in the field amplitude (as in Figures 5, 6, 7). Our results are also found to be consistent with earlier reported THz SPs amplitudes for the interaction of s/p-polarized laser beams with graphene and rippled n-InSb semiconductor surface, respectively [29, 30].

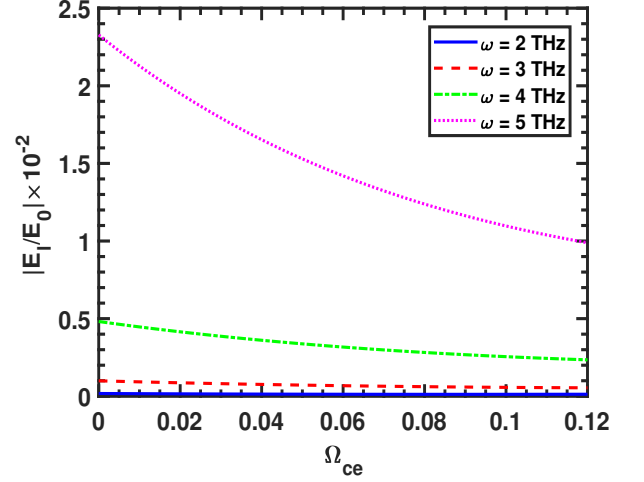


FIG. 5. Normalized THz SMPs field amplitude $|E_l/E_0|$ versus Ω_{ce} for different THz frequency $\omega = 2$ THz, 3 THz, 4 THz and 5 THz at a fixed value of graphene Fermi energy $E_F = 120$ meV and incident angle $\theta = 82.83^\circ$. Other parameters are ripple height $h = 10\mu m$, illumination length $d = 10\mu m$, and plasma frequency $\omega_p = 9.38$ THz.

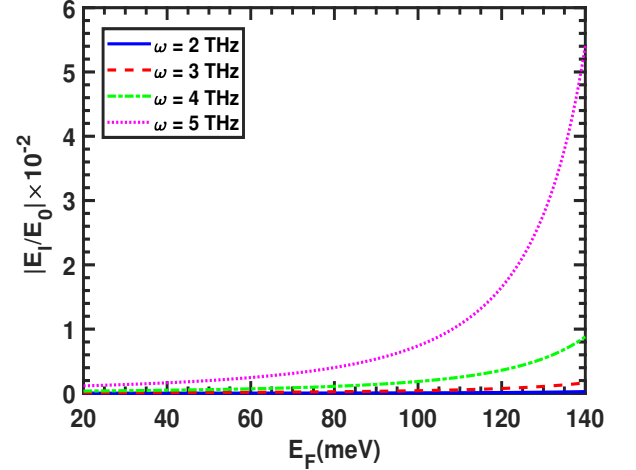


FIG. 6. Normalized THz SMPs field amplitude $|E_l/E_0|$ versus graphene Fermi energy for different THz frequency $\omega = 2$ THz, 3 THz, 4 THz and 5 THz at a fixed value of incident angle $\theta = 82.83^\circ$ and frequency $\Omega_{ce} = 0.04$. Other parameters are same as in Fig.5.

V. CONCLUSION

In this work, we have explored the excitation of THz SMPs wave by analyzing the interaction of a p-polarized laser beam obliquely incident on a graphene-n-InSb semiconductor rippled surface in the presence/absence of an external magnetic field. The possibility of generation of THz SMPs has been assessed within the frequency range of $\sim 2 - 5$ THz, with the graphene Fermi energy spanning from 20 meV to 140 meV, and the external magnetic field from 0 to 896.5 Gauss. Some important conclusions may be drawn from our results:

(i). The amplitude of normalized THz SMPs wave grows as graphene Fermi energy increases (Figure 6) because it is found from the dispersion curve of THz SMPs (Figure 3) that the normalized propagation constant $K_z = k_z c / \omega_p$ increases with increase in graphene Fermi energy. When $k_z \gg \omega/c$,

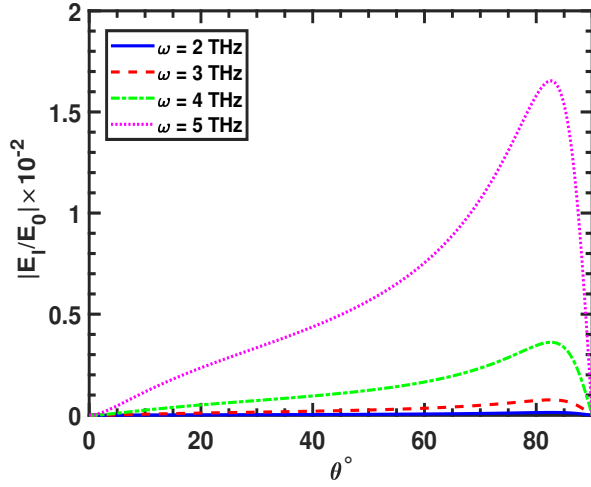


FIG. 7. Normalized THz SMPs field amplitude $|E_l/E_0|$ versus incident laser angle θ for different THz frequency $\omega = 2$ THz, 3 THz, 4 THz and 5 THz at a fixed value of $E_F = 120$ meV and $\Omega_{ce} = 0.04$. Other parameters are same as in Fig.5.

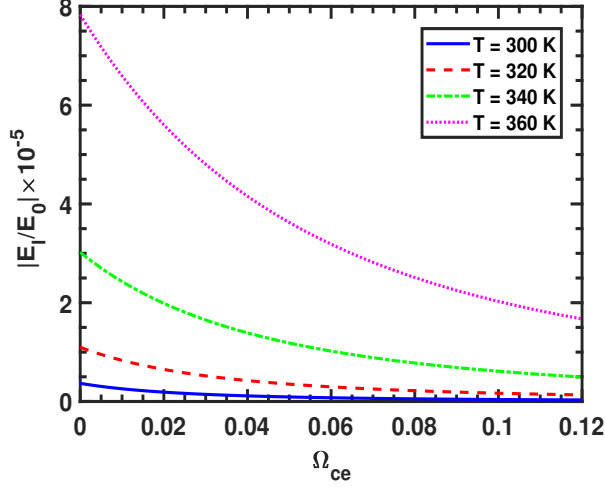


FIG. 8. Normalized THz SMPs field amplitude $|E_l/E_0|$ versus frequency Ω_{ce} for different values of n-type semiconductor temperature $T = 300$ K, 320 K, 340 K and 360 K at a fixed value of $E_F = 120$ meV, THz frequency $\omega = 5$ THz and incident laser angle $\theta = 82.83^\circ$. Other parameters are same as in Fig.5.

the terms in Eq.(14) simplify as follows: $\alpha_1 \approx k_z$, $\alpha_2 \approx k_z$ and in the coupling term $-k_z^2$ dominates. Consequently, the amplitude of normalized THz SMPs can be expressed as

$$\left| \frac{E_l}{E_0} \right| = \left| \frac{i\omega_p^2 k_z^2 \times T_{lr} h d}{2\omega \epsilon_{xx} (2 + \beta_1^2 + \beta_2^2)} \left[i(\beta_1^* + \beta_2^*) \tilde{v}_x - 2\tilde{v}_z \right] \right|. \quad (15)$$

From Eq.(15), it is evident that $|E_l/E_0| \propto k_z^2$. Therefore, the amplitude of the THz SMPs grows as the normalized propagation constant K_z increases.

(ii). The field strength of THz SMPs wave grows as THz frequency ω increases (Figure 5 and Figure 6) because required ripple wave-number $Q = qc/\omega_p$ increases (Figure 4) with increase in THz frequency Ω .

(iii). The field amplitude of THz SMPs wave grows (Figure 8) as the temperature of the n-InSb semiconductor increases. This enhancement occurs because higher temperatures lead to an increase in the electron charge density n_0 , which in turn increases $\omega_p \propto \sqrt{n_0} \propto \sqrt{T^{3/2} \exp(0.26/k_B T)}$ [58, 59]. As a result, the amplitude of THz SMPs wave grows which is consistent with Eq.(14); i.e., $|E_l/E_0| \propto \omega_p^2 \propto T^{3/2} \exp(0.26/k_B T)$.

(iv). The amplitude of generated THz SMPs wave reaches its maximum (Figure 7) at a normalized THz frequency where SMPs resonance occurs.

Our approach introduces a few extra tunable parameters such as graphene Fermi energy E_F , n-InSb semiconductor's temperature T , external magnetic field B_0 and incidence angle of laser θ for controlling the amplitude of THz SMPs wave. This scheme can be used to the development of actively tunable THz plasmonic devices, which hold significant potential for a wide spectrum of applications in communication technologies, sensing systems, and detection devices [62–65].

VI. AUTHOR DECLARATIONS

A. Conflict of interest

The authors have no conflicts to disclose.

B. Author Contributions

Rohit Kumar Srivastav (RKS) and Mrityunjay Kundu (MK) have developed the work. Figures and the original draft of the manuscript have been prepared by RKS. Review and editing of the final manuscript have been done by MK.

VII. DATA AVAILABILITY

The data that support the findings of this study are available from the corresponding author upon reasonable request.

VIII. REFERENCES

- [1] M. Tonouchi, Cutting-edge terahertz technology, *Nature photonics* **1**, 97 (2007).
- [2] P. U. Jepsen, D. G. Cooke, and M. Koch, Terahertz spectroscopy and imaging—modern techniques and applications, *Laser & Photonics Reviews* **5**, 124 (2011).
- [3] X.-C. Zhang, J. Xu, *et al.*, *Introduction to THz wave photonics*, Vol. 29 (Springer, 2010).
- [4] J. Wekalao, A. K. U, H. B. Albargi, M. Jalalah, A. H. Almagani, and A. Armghan, Graphene and gold metasurface-based terahertz surface plasmon resonance sensor for explosive detection, *Plasmonics* **19**, 3131 (2024).
- [5] D. A. Bandurin, D. Svintsov, I. Gayduchenko, S. G. Xu, A. Principi, M. Moskotin, I. Tret'yakov, D. Yagodkin, S. Zhukov, T. Taniguchi, *et al.*, Resonant terahertz detec-

- tion using graphene plasmons, *Nature communications* **9**, 5392 (2018).
- [6] G. Tzydynzhapov, P. Gusikhin, V. Muravev, A. Dremin, Y. Nefyodov, and I. Kukushkin, New real-time sub-terahertz security body scanner, *Journal of Infrared, Millimeter, and Terahertz Waves* **41**, 632 (2020).
- [7] H.-B. Liu, H. Zhong, N. Karpowicz, Y. Chen, and X.-C. Zhang, Terahertz spectroscopy and imaging for defense and security applications, *Proceedings of the IEEE* **95**, 1514 (2007).
- [8] L. Zhang, M. Zhang, and A. S. Mujumdar, Terahertz spectroscopy: A powerful technique for food drying research, *Food Reviews International* **39**, 1733 (2023).
- [9] M. Koch, D. M. Mittleman, J. Ornik, and E. Castro-Camus, Terahertz time-domain spectroscopy, *Nature Reviews Methods Primers* **3**, 48 (2023).
- [10] J. Wekalao, H. B. Albargi, S. K. Patel, M. Jalalah, A. H. Al-mawgani, R. Manvani, and A. Armghan, Terahertz optical ultrasensitive glucose detection using graphene and silver surface plasmon resonance metasurfaces for biomedical applications, *Plasmonics* <https://doi.org/10.1007/s11468-024-02278-5> (2024).
- [11] M. Gezimati and G. Singh, Advances in terahertz technology for cancer detection applications, *Optical and Quantum Electronics* **55**, 151 (2023).
- [12] M. Gezimati and G. Singh, Terahertz imaging and sensing for healthcare: current status and future perspectives, *IEEE Access* **11**, 18590 (2023).
- [13] A. Gong, Y. Qiu, X. Chen, Z. Zhao, L. Xia, and Y. Shao, Biomedical applications of terahertz technology, *Applied Spectroscopy Reviews* **55**, 418 (2020).
- [14] V. K. Shukla, M. Singh, S. Hussain, and R. K. Singh, External static electric field assisted THz radiation generation via optical rectification of secant hyperbolic laser pulse in a plasma, *Physics of Plasmas* **31**, 083301 (2024).
- [15] M. Hedegaard Kristensen, E. Herault, D. Zhai, E. Skovsen, and J.-L. Coutaz, Terahertz generation through optical rectification in reflection, *Journal of Applied Physics* **133**, 173103 (2023).
- [16] L. Guiramand, J. Nkeck, X. Ropagnol, T. Ozaki, and F. Blanchard, Near-optimal intense and powerful terahertz source by optical rectification in lithium niobate crystal, *Photonics Research* **10**, 340 (2022).
- [17] A. Singh, K. Gopal, D. Gupta, M. Kundu, and P. Varshney, Laser beat-wave interaction with electron-hole plasmas relevant to terahertz field generation, *Indian Journal of Physics* **98**, 383 (2024).
- [18] D.-S. Zhang, X.-R. Hong, X.-B. Zhang, R.-A. Tang, and B.-S. Xie, Generation of the vortex terahertz radiation by the interaction of two-color laguerre-gaussian laser with plasmas in the presence of a static magnetic field, *Physics of Plasmas* **31**, 073107 (2024).
- [19] Z. Ghayemmoniri, R. N. Siahmazgi, and S. Jafari, Terahertz radiation generation driven by beating of chirped laser pulses in single-walled carbon nanotubes by applying tapered magnetic field, *The European Physical Journal D* **77**, 48 (2023).
- [20] A. Di Gaspare, C. Song, C. Schiattarella, L. H. Li, M. Salih, A. Giles Davies, E. H. Linfield, J. Zhang, O. Balci, A. C. Ferrari, *et al.*, Compact terahertz harmonic generation in the reststrahlenband using a graphene-embedded metallic split ring resonator array, *Nature Communications* **15**, 2312 (2024).
- [21] P. Varshney, A. Singh, A. Upadhyay, M. Kundu, and K. Gopal, Effect of laser intensity redistribution on semiconductor plasma based thz emission, *Optik* **250**, 168353 (2022).
- [22] A. A. M. Choobini and F. M. Aghamir, Variable laser profiles and polarization states in the wave-mixing scheme for the generation of thz radiation in collisional-magnetized clustered-plasma, *Physics of Plasmas* **30** (2023).
- [23] W. Sun, X. Wang, and Y. Zhang, Terahertz generation from laser-induced plasma, *Opto-Electronic Science* **1**, 220003 (2022).
- [24] G. Y. Slepian, S. Maksimenko, V. Kalosha, A. Gusakov, and J. Herrmann, High-order harmonic generation by conduction electrons in carbon nanotube ropes, *Physical Review A* **63**, 053808 (2001).
- [25] G. H. Welsh, N. T. Hunt, and K. Wynne, Terahertz-pulse emission through laser excitation of surface plasmons in a metal grating, *Phys. Rev. Lett.* **98**, 026803 (2007).
- [26] J. Y. Hua, X. B. Zhang, M. Chen, S. M. Weng, Y. P. Chen, and Z. M. Sheng, Enhanced terahertz radiation generated by intense laser interaction with a two-layer thin solid target, *Phys. Rev. Accel. Beams* **27**, 081301 (2024).
- [27] A. Chamoli, D. N. Gupta, and V. Kumar, Terahertz surface plasmon generation from laser interaction with a magnetized metallic surface, *Plasmonics* <https://doi.org/10.1007/s11468-024-02358-6> (2024).
- [28] S. Vij, Radiation generation from an array of magnetized anharmonic carbon nanotubes, *Journal of Applied Physics* **136**, 083108 (2024).
- [29] P. Kumar, M. Kumar, and V. Tripathi, Linear mode conversion of terahertz radiation into terahertz surface magnetoplasmons on a rippled surface of magnetized n-insb, *Optics letters* **41**, 1408 (2016).
- [30] R. K. Srivastav and A. Panwar, Linear mode conversion of terahertz radiation into terahertz surface plasmon wave over a graphene-free space interface, *International Journal of Materials Research* **114**, 572 (2023).
- [31] K. S. Novoselov, A. K. Geim, S. V. Morozov, D. Jiang, M. I. Katsnelson, I. V. Grigorieva, S. V. Dubonos, and A. A. Firsov, Two-dimensional gas of massless dirac fermions in graphene, *nature* **438**, 197 (2005).
- [32] J. Tao, L. Wu, and G. Zheng, Graphene surface-polariton in-plane cherenkov radiation, *Carbon* **133**, 249 (2018).
- [33] P. A. D. Gonçalves and N. M. Peres, *An introduction to graphene plasmonics* (World Scientific, 2016).
- [34] S. Huang, C. Song, G. Zhang, and H. Yan, Graphene plasmonics: physics and potential applications, *Nanophotonics* **6**, 1191 (2017).
- [35] P.-Y. Chen, C. Argyropoulos, M. Farhat, and J. S. Gomez-Diaz, Flatland plasmonics and nanophotonics based on graphene and beyond, *Nanophotonics* **6**, 1239 (2017).
- [36] S. A. Mikhailov and K. Ziegler, New electromagnetic mode in graphene, *Physical review letters* **99**, 016803 (2007).
- [37] T. Low, A. Chaves, J. D. Caldwell, A. Kumar, N. X. Fang, P. Avouris, T. F. Heinz, F. Guinea, L. Martin-Moreno, and F. Koppens, Polaritons in layered two-dimensional materials, *Nature materials* **16**, 182 (2017).
- [38] D. A. Kuzmin, I. V. Bychkov, V. G. Shavrov, and L. N. Kotov, Transverse-electric plasmonic modes of cylindrical graphene-based waveguide at near-infrared and visible frequencies, *Scientific reports* **6**, 26915 (2016).
- [39] D. Teng, K. Wang, and Z. Li, Graphene-coated nanowire waveguides and their applications, *Nanomaterials* **10**, 229 (2020).
- [40] I. Moiseenko, V. Popov, and D. Fateev, Terahertz amplification and lasing by using transverse electric modes in a two-layer-graphene-dielectric waveguide structure with direct current, *Journal of Physics: Condensed Matter* **35**, 255301 (2023).
- [41] F. H. Koppens, D. E. Chang, and F. J. García de Abajo, Graphene plasmonics: a platform for strong light-matter inter-

- actions, *Nano letters* **11**, 3370 (2011).
- [42] F. MinovKoppensich, D. Chang, S. Thongrattanasiri, and F. G. de Abajo, Graphene plasmonics: A platform for strong light-matter interactions, *Opt. Photon. News* **22**, 36 (2011).
- [43] T.-T. Kim, H. Kim, M. Kenney, H. S. Park, H.-D. Kim, B. Min, and S. Zhang, Amplitude modulation of anomalously refracted terahertz waves with gated-graphene metasurfaces, *Advanced Optical Materials* **6**, 1700507 (2018).
- [44] T. Low and P. Avouris, Graphene plasmonics for terahertz to mid-infrared applications, *ACS nano* **8**, 1086 (2014).
- [45] L. Ye, Y. Chen, G. Cai, N. Liu, J. Zhu, Z. Song, and Q. H. Liu, Broadband absorber with periodically sinusoidally-patterned graphene layer in terahertz range, *Optics express* **25**, 11223 (2017).
- [46] B. Yao, Y. Liu, S.-W. Huang, C. Choi, Z. Xie, J. Flor Flores, Y. Wu, M. Yu, D.-L. Kwong, Y. Huang, *et al.*, Broadband gate-tunable terahertz plasmons in graphene heterostructures, *Nature Photonics* **12**, 22 (2018).
- [47] D. Wu, J. Tian, L. Li, and R. Yang, Plasmon induced transparency and refractive index sensing in a new type of graphene-based plasmonic waveguide, *Optics Communications* **412**, 41 (2018).
- [48] R. Hao, J. Jiao, X. Peng, Z. Zhen, R. Dagarbek, Y. Zou, and E. Li, Experimental demonstration of a graphene-based hybrid plasmonic modulator, *Optics letters* **44**, 2586 (2019).
- [49] X. Hu and J. Wang, Ultrabroadband compact graphene–silicon tm-pass polarizer, *IEEE Photonics Journal* **9**, 1 (2017).
- [50] R. K. Srivastav and A. Panwar, Resonant excitation of terahertz surface magnetoplasmons by optical rectification over a rippled surface of n-type indium antimonide, *Journal of Plasma Physics* **90**, 905900106 (2024).
- [51] F. Liu, P. Li, H. An, P. Peng, B. McLean, and F. Ding, Achievements and challenges of graphene chemical vapor deposition growth, *Advanced Functional Materials* **32**, 2203191 (2022).
- [52] M. Saeed, Y. Alshammari, S. A. Majeed, and E. Al-Nasrallah, Chemical vapour deposition of graphene—synthesis, characterisation, and applications: A review, *Molecules* **25**, 3856 (2020).
- [53] F. Liu, C. Qian, and Y. D. Chong, Directional excitation of graphene surface plasmons, *Optics express* **23**, 2383 (2015).
- [54] Z. Yu, G. Veronis, Z. Wang, and S. Fan, One-way electromagnetic waveguide formed at the interface between a plasmonic metal under a static magnetic field and a photonic crystal, *Physical review letters* **100**, 023902 (2008).
- [55] F. J. García de Abajo, Graphene plasmonics: challenges and opportunities, *Acs Photonics* **1**, 135 (2014).
- [56] L. Xu, Y. Shen, L. Gu, Y. Li, X. Deng, Z. Wei, J. Xu, and J. Cao, Optical strong coupling in hybrid metal-graphene metamaterial for terahertz sensing, *Chinese Physics B* **30**, 118702 (2021).
- [57] J. Brion, R. Wallis, A. Hartstein, and E. Burstein, Theory of surface magnetoplasmons in semiconductors, *Physical Review Letters* **28**, 1455 (1972).
- [58] H. Jing, Y. Wei, J. Duan, J. Hao, W. Zhao, Z. Qu, J. Wang, and B. Zhang, Thermally and magnetically controlled dual-band terahertz metamaterial absorber based on insb, *Optical Materials* **129**, 112311 (2022).
- [59] P. Gao, J. Sun, W. Li, C. Su, Z. Sun, F. Xia, K. Zhang, L. Dong, and M. Yun, Multifunctional and dynamically tunable coherent perfect absorber based on insb and graphene metasurface, *Results in Physics* **52**, 106797 (2023).
- [60] D. B. Singh and V. K. Tripathi, Surface plasmon excitation at second harmonic over a rippled surface, *Journal of Applied Physics* **102**, 083301 (2007).
- [61] C. S. Liu and V. K. Tripathi, Kinetic magnetoplasmons in graphene and their excitation by laser, *Journal of Nanophotonics* **11**, 036015 (2017).
- [62] K. Liu, Y. Feng, C. Han, B. Chang, Z. Chen, Z. Xu, L. Li, B. Zhang, Y. Wang, and Q. Xu, High-speed 0.22 thz communication system with 84 gbps for real-time uncompressed 8k video transmission of live events, *Nature Communications* **15**, 8037 (2024).
- [63] I. F. Akyildiz, C. Han, Z. Hu, S. Nie, and J. M. Jornet, Terahertz band communication: An old problem revisited and research directions for the next decade, *IEEE Transactions on Communications* **70**, 4250 (2022).
- [64] A.-C. Samaha, J. Doumani, T. E. Krizzell, H. Xu, A. Baydin, P. M. Ajayan, M. E. Tahchi, and J. Kono, Graphene terahertz devices for sensing and communication, *Small* <https://doi.org/10.1002/sml.202401151> (2024).
- [65] H. Liu, X. Wang, C. Chen, H. Cui, F. Cui, Y. Dai, P. Gao, S. Duan, Z. Gao, and T. Zhou, Terahertz polarization sensing for influenza a virus based on plasmonic metasurface, *Journal of Optics* **26**, 095102 (2024).